Device Physics of an Optoelectronic Integrated Wavelength Converter

J. Piprek,[i] V. Lal, J. Hutchinson,[*] J. Henness, A. Tauke Pedretti, M. Dummer, and L. Coldren

Electrical and Computer Engineering Department
University of California, Santa Barbara, CA 93106
[*] Intel Corporation, Portland, OR

ABSTRACT

An InP-based tunable wavelength converter is investigated which monolithically combines a waveguide photodetector with a sampled-grating distributed Bragg reflector laser diode. We employ advanced device simulation to study internal physical mechanisms and performance limitations. Our three-dimensional finite-element model self-consistently combines carrier transport, optical waveguiding, and nanoscale many-body theory to accurately account for optical transitions within the quantum wells. Good agreement with measurements is achieved. The validity of several model simplification options is discussed.

Keywords: Optoelectronic integrated circuit, wavelength converter, semiconductor optical amplifier, many-body theory, three-dimensional device simulation, rate equation model

1. INTRODUCTION

Wavelength converters are of interest for wavelength-division multiplexing (WDM) fiber-optic communication systems to transfer signals from one channel to another. We investigate a monolithic InP-based tunable wavelength converter which combines a waveguide photodetector with a sampled-grating distributed Bragg reflector (SGDBR) laser diode.[1] Table 1 lists the epitaxial structure including the multi-quantum well (MQW) active region. Figure 1 shows a schematic layout of the entire converter. The receiver integrates signal pre-amplification by a semiconductor optical amplifier (SOA) and signal detection by a waveguide photodiode (WPD). The optical signal is converted into an electrical signal that directly modulates the tunable SGDBR laser diode which is integrated with a semiconductor optical amplifier for signal enhancement. Further experimental details are given elsewhere.[2]

Layer	Material	Thickness nm	Doping 10^{18} cm^{-3}
p-contact	InGaAs	100	30 (p)
upper cladding	InP	1600	1 (p)
upper cladding	InP	200	0.3 (p)
doping setback	InP	50	-
quantum barrier (8x)	$In_{0.685}Ga_{0.315}As_{0.595}P_{0.405}$	8	-
quantum well (7x)	$In_{0.685}Ga_{0.315}As_{0.864}P_{0.136}$	6.5	-
etch stop	InP	10	-
waveguide	$In_{0.612}Ga_{0.338}As_{0.728}P_{0.272}$	350	0.1 (n)
lower cladding	InP	1400	1 (n)
etch stop / n-contact	InGaAs	100	1 (n)
Buffer	InP	1000	-

Tab. 1 Epitaxial layer sequence of the monolithic device.

[i] Corresponding author, e-mail: piprek@ieee.org

Optoelectronic Integrated Circuits VII, edited by Louay A. Eldada, El-Hang Lee, Proc. of SPIE Vol. 5729
(SPIE, Bellingham, WA, 2005) · 0277-786X/05/$15 · doi: 10.1117/12.584570

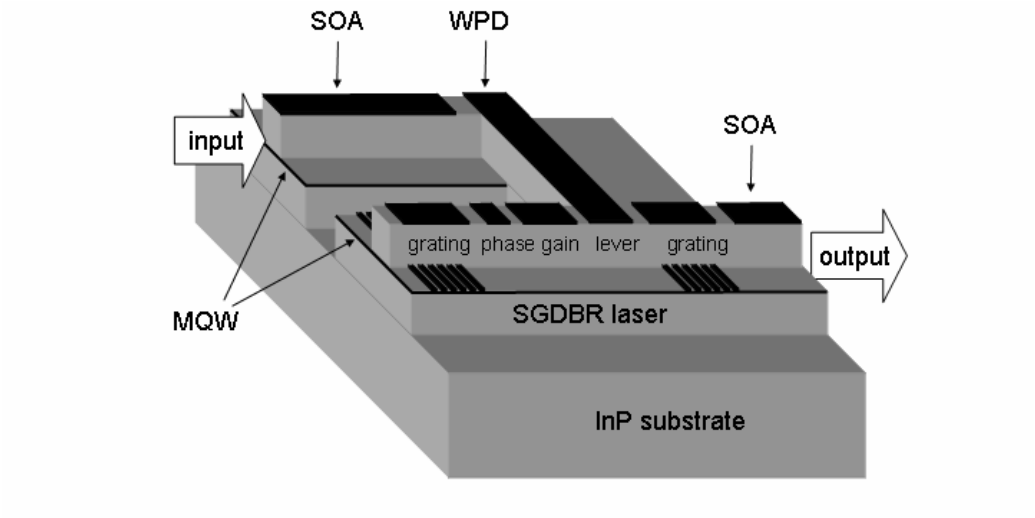

Fig. 1: Schematic view of the optoelectronic integrated wavelength converter.

We here analyze internal physical processes of this device using advanced numerical simulation that is in good agreement with our measurements. Section 2 compares different models for optical transitions within the quantum wells. Section 3 outlines the three-dimensional (3D) device model and introduces a more simple rate equation model for the amplifier. Section 4 compares the simulation results from both models to SOA saturation measurements.

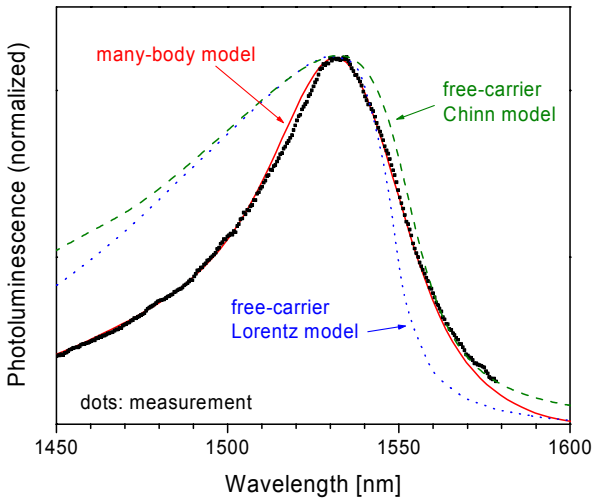

Fig. 2: Comparison of measured and calculated photoluminescence spectra.

2. QUANTUM WELL MODELING

The accurate modeling of quantum well properties, in particular the optical transition rates (spontaneous emission, gain, absorption) are prerequisite for a realistic simulation of the wavelength converter. We initially employed a simple free-carrier model based on 4x4 kp band structure calculations and using a Lorentz energy broadening function.[3] However, this approach did not give consistent agreement with experimental results.[4] A comparison to the measured photoluminescence spectrum is shown in Fig. 2 revealing discrepancies on both sides of the spectrum. The energy broadening model by Chinn et al.[5] is considered an improvement over the Lorentz model as it describes the low-energy tail of the Lorentz function by a more appropriate Gaussian function. Indeed, this spectrum shows better agreement for

low energies in Fig. 2 (dashed line), however, both free-carrier models deviate substantially from the measurement at high energies. Thus, energy broadening effects by many-body interactions require more careful consideration using advanced many-body theory.[6] This many-body model provides excellent agreement across the entire spectrum (solid curve in Fig. 2) which is of paramount importance for predictions of our device performance for all possible wavelengths (1525 nm - 1565 nm). Carrier-carrier and carrier-phonon interactions seem to have a non-trivial influence on the optical transition probabilities and cannot be represented by simple broadening functions.

Figure 3 plots calculated gain vs. density characteristics for different wavelengths. In agreement with experimental observations, the many-body model (solid line) gives almost constant gain across the wavelength range of interest. The free-carrier Chinn model (dashed lines) shows considerable gain variations within the same wavelength range. It comes close to the many-body results only for wavelengths near 1553 nm.

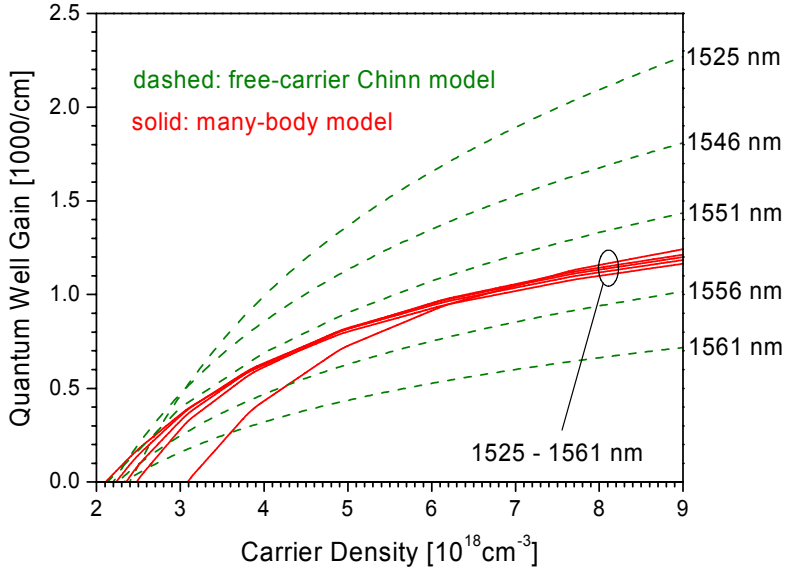

Fig. 3: Gain vs. carrier density characteristics from both models at different wavelength.

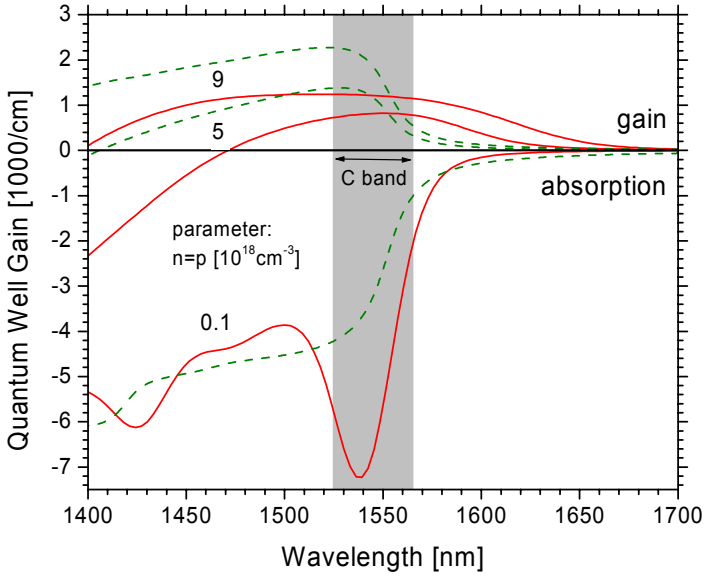

Fig. 4: Gain spectra from both models at different carrier densities.

Full gain/absorption spectra are compared in Fig. 4 for three carrier densities. At higher densities, the spectra cross each other at 1552 nm and 1554 nm, respectively, and reasonable agreement of device simulations can only be expected in close proximity to those wavelengths. Near the short-wavelength boundary of the C-band, the two models differ by a factor of two. With very low quantum well carrier densities, as in photodetectors, the absorption spectra also show significant differences. While the calculated bulk absorptions at higher energies are relatively close, the main differences occur near the band edge due to exciton transitions. Such electron-hole interactions are fully considered in the many-body model and cause a strong absorption peak, which is missing in the free-carrier model.

3. DEVICE SIMULATION

We now implement the precalculated many-body spectra into the 3D device simulation code PICS3D.[7] This software self-consistently combines the carrier transport (including Fermi statistics and thermionic emission) with optical wave-guiding. Details of the 3D model and of the many-body spectra integration are published elsewhere.[8] This novel simulation approach results in excellent agreement with a variety of device measurements, as reported earlier. [9,10]

In the following, we outline a more simple rate equation model for the SOA which will be shown to give good agreement with the 3D model as long as the same many-body spectra are implemented. The carrier rate equation for the MQW active region is given by

$$\frac{\partial N(t)}{\partial t} = \frac{\eta_i I}{qV} - (AN + BN^2 + CN^3) - \frac{\Gamma}{wd\hbar}\frac{g(N,\omega_s)}{\omega_s}P_s(t)$$

where

N	is the electron density (assumed equal to hole density)
η_i	is the injection efficiency
I	is the injected current
V	is the volume of the active region
A,B,C	are the recombination parameters
Γ	is the overlap of the optical mode with the active material
w,d	are the active region width and height resp.
P_s	is the input signal power
ω_s	is the signal frequency
g	is the material gain at carrier density N and frequency ω

This type of a description works well for a resonant or gain-clamped SOA, but for a traveling wave type SOA where there are no facet reflections, carrier density and power distributions are non-uniform along the length of the SOA, and models that approximate the entire SOA with a single average carrier density do not work well. For this reason, we break our SOA region into a number of much smaller elements, within which we can approximate the carrier density as uniform. This approach is depicted in Fig 5.

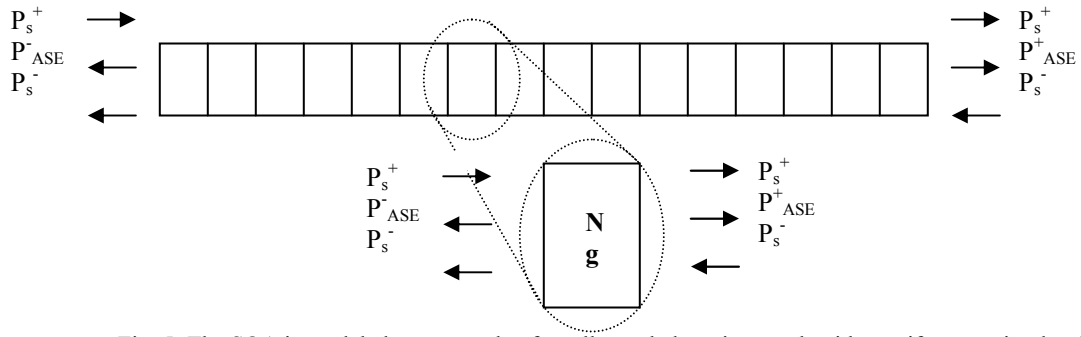

Fig. 5: The SOA is modeled as a cascade of small coupled sections each with a uniform carrier density

Each section of the SOA can then be described using the following three equations:

$$\frac{\partial N(z,t)}{\partial t} = \frac{\eta_i J}{qd} - (AN + BN^2 + CN^3) - \frac{\Gamma}{wd\hbar}\left[\sum_k \frac{g(N,\omega_s)}{\omega_s} P_s(z,t) + \int \frac{g(N,\omega)}{\omega}(P^{ASE+} + P^{ASE-})d\omega\right]$$

$$\frac{1}{v_g}\frac{\partial P_s^{\pm}}{\partial t} \pm \frac{\partial P_s^{\pm}}{\partial z} = \left[\Gamma g(N,\omega_s) - \alpha_i\right]P_s^{\pm} \qquad \forall k$$

$$\frac{1}{v_g}\frac{\partial P^{ASE\pm}}{\partial t} \pm \frac{\partial P^{ASE\pm}}{\partial z} = \left[\Gamma g(N,\omega) - \alpha_i\right]P^{ASE\pm} + \beta R_{sp}(N,\omega)A\hbar\omega \quad \forall \omega$$

where,

$P^{ASE+/-}$	is the power spectral density of the ASE traveling in the + or – direction
J	is current density in the particular section of the SOA
v_g	is the signal group velocity
β	is the spontaneous emission factor
R_{sp}	is the spontaneous emission rate

The first equation describes the rate of change of electron/hole density in the given SOA section, which depends on the signal power and the amplified spontaneous emission (ASE) power present in the section. The summation is over all signals propagating in both the positive and negative direction, and the ASE is integrated over its entire spectrum. The second equation describes the propagation of the signal across a gain medium. Finally, the third equation describes the evolution of the ASE power spectral density. The βR_{sp} term is the generated spontaneous emission that couples into the guided modes of the SOA. For index guided traveling wave SOAs, that do not have resonant modes in the longitudinal direction, β is given by

$$\beta = (2\pi n)^{-2}\frac{\lambda_o^2}{S_o}$$

with S_o being the optical mode area. The equations can be easily solved iteratively to compute the gain, signal, and ASE in different sections of the SOA. However, ASE is found negligible in our example.

4. COMPARISON TO AMPLIFIER MEASUREMENTS

We now compare the results of both device models, including many-body spectra, to saturation measurements on our amplifier structure. The SOA is 600 μm long and its ridge width is 3 μm. The same parameters are used in both models.[8] The injection efficiency η_i=0.82 and the optical confinement factor Γ = 0.06 are extracted from the full 3D simulation. The internal optical loss is assumed as α_i = 10/cm, additional intervalence band absorption is neglected here. Figure 6 plots the calculated SOA output power vs. input power in comparison to the measurement (dots).

The agreement between both device models is surprisingly good, indicating that the quantum well recombination processes dominate the SOA performance. The carrier transport to the MQW as well as the carrier distribution within the MQW do not seem very important, as both are neglected in the rate equation model. Only slight deviations are observed at higher power. The full 3D simulation gives slightly stronger non-linearity which may be attributed to differences in the recombination rates. While Auger coefficients and SRH lifetimes are identical in both models, the spontaneous recombination rate is computed differently. The rate equation model uses the common coefficient B = 10^{-10} cm^3/s whereas PICS3D integrates the many-body spectra for the spontaneous emission. At low power, the full 3D model gives a slightly higher gain than the rate equation model. This is identified as numerical artifact which can be avoided by reducing the initial input power of the PICS3D simulation.

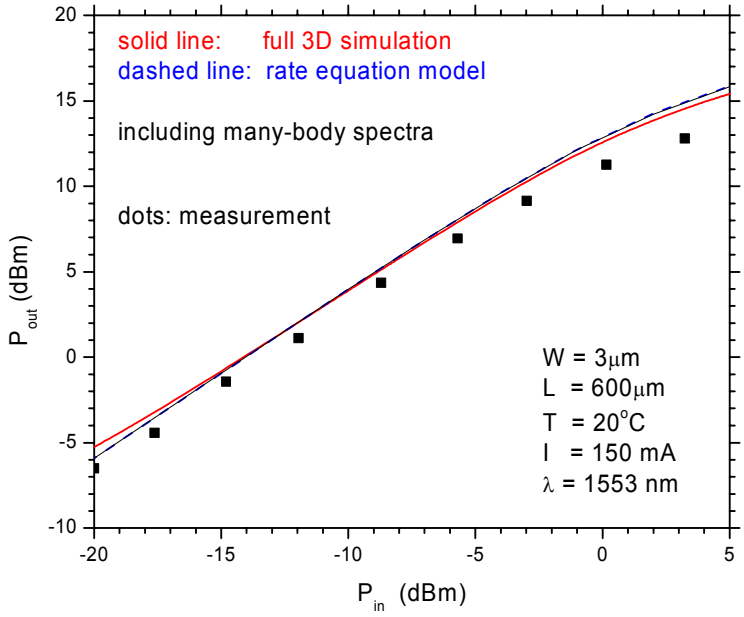

Fig. 6: Amplifier output power vs. input power at 8.3 kA/cm^2 current density.

By employing advanced many-body theory, both models give good agreement with the measurement in Fig. 6. The remaining small deviation can have multiple reasons, e.g., additional optical losses and/or self-heating of the device, which is neglected in both models. 3D thermal simulations show an active region temperature rise of about 15K at 150mA current assuming a thermal resistance of 100 K/W for substrate and heat sink.

5. SUMMARY

Different simulation approaches are compared to achieve a realistic representation of internal device physics in our wavelength converter. The application of many-body theory to the calculation of quantum well optical spectra is identified as most essential element of the model. Carrier transport and distribution effects seem less important.

ACKNOWLEDGMENT

This research project was sponsored by the Semiconductor Research Corporation (Award 2001-NJ-968) and by the Intel Corporation. Supercomputer calculations of the many-body spectra have been performed by Nonlinear Control Strategies, Inc., Tucson, AZ.

REFERENCES

[1] V. Jayaraman, A. Mathur, L. A. Coldren, and P. D. Dapkus, "Theory, design, and performance of extended tuning range in sampled grating DBR lasers," IEEE J. Quantum Electron., vol. 29, pp. 1824–1834, 1993.

[2] J. Hutchinson, J. Barton, M. Masanovic, M. Sysak, J. Henness, L. Johansson, D. Blumenthal, and L. A. Coldren, "Monolithically integrated InP-based tunable wavelength conversion." In: *Physics and Simulation of Optoelectronic Devices XII,* SPIE Proc. Vol. 5349, pp. 176-184, 2004.

[3] S. L. Chuang, *Physics of Optoelectronic Devices,* Wiley, New York 1995.

[4] J. Piprek, N. Trenado, J. Hutchinson, J. Henness, and L. A. Coldren, "3D Simulation of an integrated wavelength converter." In: *Physics and Simulation of Optoelectronic Devices XII,* SPIE Proc. Vol. 5349, pp. 185-196, 2004.

[5] S. Chinn, P. Zory, and A. Reisinger, IEEE J. Quantum Electron., vol. 24, pp. 2191-2214 (1988)

[6] S.W. Koch, J. Hader, A. Tränhardt, and J.V. Moloney, "Gain and Absorption: Many-Body Effects," Chapter 1 in: *Optoelectronic Devices – Advanced Simulation and Analysis*, J. Piprek (ed.), Springer Verlag, New York, 2004.

[7] PICS3D by Crosslight Software (www.crosslight.com)

[8] J. Piprek, S. Li, P. Mensz, and J. Hader, "Monolithic Wavelength Converter," Chapter 14 in: *Optoelectronic Devices – Advanced Simulation and Analysis*, J. Piprek (ed.), Springer Verlag, New York, 2004.

[9] J. Piprek, J. Hutchinson, J. Henness, L. Coldren, and J. Hader; "Many-Body Effects on InP-based Optoelectronic Wavelength Converters for WDM Applications" (postdeadline) 4th IEEE/LEOS Int. Conf. on *Numerical Simulation of Optoelectronic Devices*, Santa Barbara, August 2004.

[10] J. Piprek, J. Hutchinson, J. Henness, M. Masanovic, and L. A. Coldren; "Saturation Analysis of a Monolithic Wavelength Converter," in: *Physics and Applications of Optoelectronic Devices*, SPIE Proc. 5594, pp. 102-109, 2004.